Received: 23 October 2020 | Accepted: 11 December 2020

DOI: 10.1049/gtd2.12110

IET Generation, Transmission & Distribution

The Institution of Engineering and Technology WILEY

ORIGINAL RESEARCH PAPER

A non-singular fast terminal sliding mode control scheme for residual current compensation inverters in compensated distribution networks to mitigate powerline bushfires

Tushar Kanti Roy[1,2] | **Md Apel Mahmud**[2] | **A. B. M. Nasiruzzaman**[2] | **Md Abdul Barik**[3] | **Amanullah Maung Than Oo**[2]

[1] Department of Electronics and Telecommunication Engineering, Rajshahi University of Engineering and Technology, Rajshahi 6204, Bangladesh

[2] Electrical Power & Energy Systems Research Lab (EPESRL), School of Engineering, Deakin University, Waurn Ponds, VIC 3216, Australia

[3] AusNet Services, Melbourne, VIC 3006, Australia

Correspondence
Tushar Kanti Roy, Department of Electronics and Telecommunication Engineering, Rajshahi University of Engineering and Technology, Rajshahi-6204, Bangladesh.
Email: tkroy@ete.ruet.ac.bd

Abstract

This paper presents an approach to design a non-singular fast terminal sliding model controller for residual current compensation inverters in compensated distribution networks to compensate the fault current due to most commonly occurred single line-to-ground faults. The main control objective is to completely eliminate the fault current in order to mitigate the impacts of powerline bushfires. A non-singular fast terminal sliding surface is used to design the controller so that the residual current compensation inverter can quickly ensure the desired control performance without experiencing singularity problems. In this scheme, the chattering effects are minimised by replacing the discontinuous function appearing in the control law with a continuous function and the Lyapunov stability theory is utilised to demonstrate the theoretical stability of the control law. This paper also includes an overview of the non-singular terminal sliding model controller as the performance of the non-singular fast terminal sliding model controller is compared with this controller through rigorous simulation results over a range of fault currents. Simulation results clearly demonstrate the faster convergence speed of the non-singular fast terminal sliding model controller over the non-singular terminal sliding model controller for compensating the fault current and hence, mitigating powerline bushfires.

1 | INTRODUCTION

Electric faults on powerlines in distribution networks produce high fault currents which can ignite fires. One of the deadliest bushfires in the recent history of Australia caused 159 fatalities (out of total 173) that started from powerline fires on and around 7 February 2009 [1]. The 2009 Victorian Bushfires Royal Commission recommended using the technology to reduce bushfire risks with prioritising areas prone to such bushfires along with other suggestions [1]. These events led to the Victorian Government announcing Powerline Bushfire Safety Program that mandates installing the rapid earth fault current limiter (REFCL) technology in 45 high bushfire risk locations in Victoria [2]. Different parts of the world (e.g. California) are planning to use the similar technology for mitigating powerline bushfires as the REFCL works by limiting the amount of energy released through reducing the fault current within a very short period so that fires do not start. This capability is developed by installing a traditional Petersen coil in conjunction with a residual current compensation (RCC) inverter between the neutral and ground of the distribution transformer in zone sub-stations. The Petersen coil is tuned automatically with the distribution network so that the reactive component of the fault current can be minimised [3] while the RCC inverter controls both reactive and real components of this current as the coil cannot be automatically tuned to completely compensate the reactive component. Hence, the control of the RCC inverter plays a crucial role for compensating the fault current in compensated distribution networks and mitigating powerline bushfires.

Different control schemes are proposed to compensate the fault current for distribution networks. An admittance-based closed-loop control scheme is proposed in [4] that compares the locus plot of the neutral voltage to detect the faulty phase where the phase-to-ground admittance significantly varies on the faulty phase as compared to healthy phases. After the faulty phase detection, the voltage source inverter in the residual current compensator applies a voltage to the neutral point that compensates the active component of the fault current. The fault detection and full compensation method proposed in [5] relies on the calculation of the voltage drop between the supply point and the fault location. The fault is detected by utilising the principle of the travelling wave in the transmission lines. The fault current is suppressed by controlling the zero-sequence voltage. The fault current suppression methods proposed in [4, 5] is shown to reduce the fault current to a significant level during some controlled simulation environments. However, these methods need more case studies and rigorous analysis of the control schemes that were not attributed.

Proportional integral (PI) controllers have been used in [6–8] to address the fast transient response requirement as well as to reduce operational hazards arising from single-line-to-ground (SLG) faults. A cascaded H-bridge converter is used in [6] whose output compensates the fault current while relying on the calculation of the zero-sequence voltage and current including the measurement of line parameters. A distributed communication scheme is proposed in [7] that uses a PI controller to control the fault current which does not require synchronised signals for decision making as in [5]. However, the approach in [7] cannot reduce the active component of the fault current. Another PI controller as implemented in [8] uses the pulse width modulation (PWM) technique to drive a full-bridge voltage source converter for injecting current into the neutral so that the active component of the fault current can be compensated. The PI controllers in [6–8] uses a single-loop control structure and cannot track sinusoidal references and thus, these methods provide poor tracking performance.

The tracking performance is improved in [9, 10] by calculating the sinusoidal reference current that uses dual-loop control structures. In [9], the neutral voltage is controlled by the outer voltage control loop whereas the inner loop PI controller injects the current required to suppress the arc resulting from an SLG fault. A similar dual-loop control structure is used in [10] where the outer loop lag compensator generates the reference current that depends on the error of the neutral voltage and the PI controller in the inner loop regulates the current of the RCC inverter in the resonant grounded system. Combining the inner PI control loop with the outer lag compensator, the tracking performance is improved in [9, 10] for the resonant grounded system, however, the damping characteristics need to be adjusted. The damping characteristics of the controllers are controlled in [11, 12] by using proportional resonant (PR) controllers in addition to the PI controllers. An active grounding system is developed in [11] to damp the neutral-to-ground overvoltage that arises due to the asymmetry of distributed line parameters, specially the shunt capacitance and the inductance of the Petersen coil. In order to address the capacitive reactive current detection problem, an active device is presented in [12] that injects current into the neutral without large capacity reactors. PI controllers are integrated with PR controllers in [11, 12] that ensures better tracking and active damping suppression, however, these controllers are designed to act on typical low impedance faults though there are high chances of high impedance faults in the network that needs to be taken care of.

A robust H_∞ control scheme is discussed in [13] that uses a voltage source controller and provides a dynamic range of fault resistance while considering parametric uncertainties in filter parameters. In [13], the system is first order while the order of the controller is 17 and a Gram matrix-based reduction approach is used to reduce the order of the controller to seven. However, seventh-order controller is not a feasible one while considering form the perspective of the practical implementation. A model predictive control approach has been implemented in [14] that achieves a low steady-state current tracking error while maintaining fast dynamic responses and reduced switching losses. Some case studies are conducted that demonstrate the performance of the controller, however, the method in [14] uses a three-phase configuration of the arc suppression device when a single-phase can serve the purposes. The controllers in [13, 14] are linear and supports only a limited set of operating points that can be overcome by using non-linear controllers.

A non-linear backstepping control method is used in [15] by using three-phase inverters with three coils applying the principle of eliminating SLG faults. The designed controller considers the variation in the filter inductance, however, a single-phase arc suppression device can be utilised to achieve similar objectives. In [16], the backstepping control method is implemented on a single-phase arc suppression device rather than the three-phase architecture as discussed in [15]. In [16], the reference current is calculated by using a second-order phase-locked loop that over complicates the process though it effectively reduces the fault current. The methods in [15, 16] consider bounded parametric uncertainty in the filter reactance without justifying the reason of considering such parametric uncertainties. Furthermore, the complexity arising from the use of the phase-locked loop in [16] can be avoided by using the fundamental analytical expression for the neutral current when there is a SLG fault in the network. Though non-linear control schemes will be extremely useful for the fault current compensation through the RCC inverter in bushfire prone areas, these have not been widely utilised for this application. Furthermore, all existing literature so far discussed in this paper do not consider the operational standard for compensating the fault current considering the operational standards that need to be maintained to mitigate powerline bushfires. Apart from these, the RCC inverter is mostly considered as the H-bridge converter where switches experience high voltage stress and there exists high switching losses.

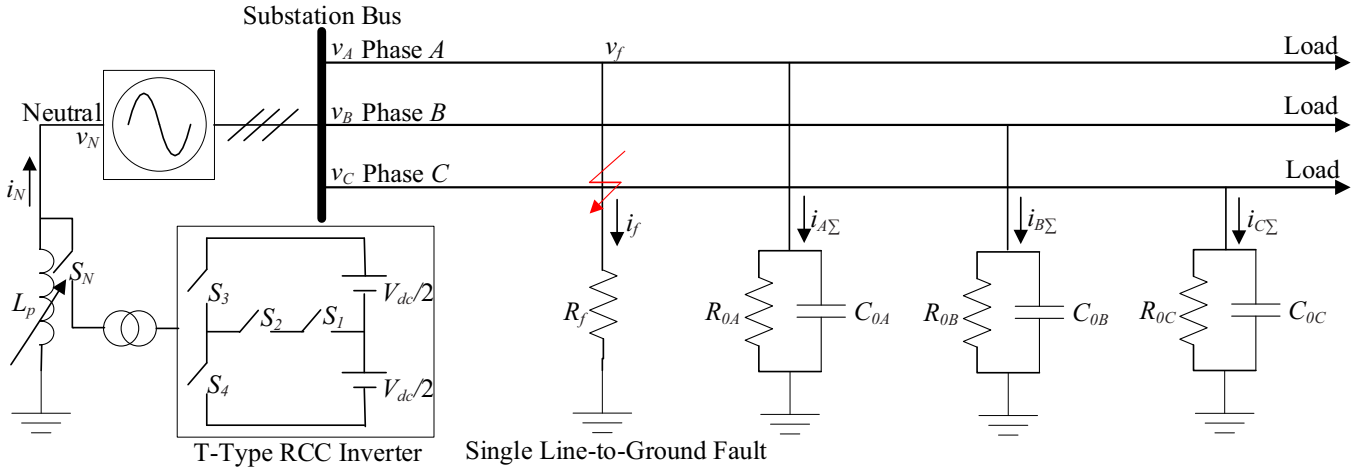

FIGURE 1 A T-type RCC inverter in a compensated power distribution system

This paper proposes a new non-singular fast terminal sliding mode controller (NFT-SMC) for the RCC inverter in a compensated distribution network which has not been used for such an application. The proposed NFT-SMC is designed based on a non-singular fast terminal sliding surface (NFT-SS) which is capable to ensure the first convergence of the tracking error without facing any singularity problems. Moreover, the switching control law using the NFT-SMC is developed in a way that the chattering effect can be overcome for which the discontinuous signum function is replaced with a continuous function. The proposed controller enables the RCC inverter to generate switching pulses in order to ensure the desired current injection at the neutral point so that the fault current is completely compensated or reduced to a value that is required for the mitigation powerline bushfires as per the regulatory framework as indicated in [17]. The performance of the proposed controller is also evaluated by satisfying the requirement for the faulty phase voltage considering both low and high impedance faults as indicated in [17]. The performance of the NFT-SMC is compared with a non-singular terminal sliding mode controller (NT-SMC) in terms of the fault current, faulty phase voltage, and injected current by considering both low and high impedance faults.

2 | DYNAMIC MODEL OF RCC INVERTERS

The compensated power distribution network in Figure 1 shows a T-type RCC inverter which is used to inject the desired current into the neutral and this paper focuses to design the switching signal for all four switches (i.e. S_1, S_2, S_3, and S_4). This RCC inverter is only activated by turning on the switch (S_N) when there is a fault in the distribution network while the step up transformer at its output is used to match the voltage with the neutral-to-ground voltage (v_N). Generally, the Petersen coil represented through an adjustable inductor (L_p) in Figure 1 is used for compensating the reactive component of the fault current (i_f) and reduce its severity. This reactive compensation is done through the resonance of L_p with the total zero-sequence capacitance of the distribution network. Figure 1 clearly shows three impedance networks (i.e. one for each phase) having a resistor (R_0) and a capacitor (C_0) with subscripts A, B, and C representing corresponding three-phases (i.e. Phases A, B, and C, respectively). The distribution network in Figure 1 is considered as a balanced one to some extents for which $R_{0A} = R_{0B} = R_{0C} = R_0$ and $C_{0A} = C_{0B} = C_{0C} = C_0$. In this section, the model is developed by considering the fault on Phase A with a fault resistance R_f as indicated in Figure 1. As a result, the fault-to-ground voltage (v_f) is basically the phase-to-ground voltage for Phase A (v_A), i.e. $v_f = v_A$. The RCC inverter compensates both active and reactive components of the fault current by enforcing the neutral current (i_N) to its reference value (i.e. $i_{N_{ref}}$) such that i_f becomes zero. Hence, it is essential to calculate this neutral current in order to determine the reference value for which i_f will be zero. The value of i_N can be calculated as

$$i_N = i_f + i_{A\sum} + i_{B\sum} + i_{C\sum} \tag{1}$$

where $i_{A\sum}$, $i_{B\sum}$, and $i_{C\sum}$ are currents flowing through zero-sequence impedance networks in Phases A, B, and C, respectively, which can be written as follows:

$$\begin{aligned} i_{A\sum} &= i_{R_{0A}} + i_{C_{0A}} \\ i_{B\sum} &= i_{R_{0B}} + i_{C_{0B}} \\ i_{C\sum} &= i_{R_{0C}} + i_{C_{0C}} \end{aligned} \tag{2}$$

where $i_{R_{0A}}$, $i_{R_{0B}}$, and $i_{R_{0C}}$ are currents flowing through R_{0A}, R_{0B}, and R_{0C}, respectively while $i_{C_{0A}}$, $i_{C_{0B}}$, and $i_{C_{0C}}$ are currents flowing through C_{0A}, C_{0B}, and C_{0C}, respectively. Since $R_{0A} = R_{0B} = R_{0C} = R_0$ and $C_{0A} = C_{0B} = C_{0C} = C_0$, the currents in Equation (2) can be written as

$$i_A \Sigma = \frac{v_A}{R_0} + C_0 \frac{dv_{C_{0A}}}{dt}$$

$$i_B \Sigma = \frac{v_B}{R_0} + C_0 \frac{dv_{C_{0A}}}{dt}$$

$$i_C \Sigma = \frac{v_C}{R_0} + C_0 \frac{dv_{C_{0A}}}{dt} \tag{3}$$

where $v_{C_{0A}}$, $v_{C_{0A}}$, and $v_{C_{0A}}$ are voltages across C_{0A}, C_{0B}, and C_{0C}, respectively, which also represent the corresponding phase-to-ground voltages, i.e. v_A, v_B, and v_C, respectively. Hence, $v_{C_{0A}} = v_A$, $v_{C_{0B}} = v_B$, and $v_{C_{0A}} = v_C$. Finally, Equation (3) can be rewritten as

$$i_A \Sigma = \frac{v_A}{R_0} + C_0 \frac{dv_A}{dt}$$

$$i_B \Sigma = \frac{v_B}{R_0} + C_0 \frac{dv_B}{dt}$$

$$i_C \Sigma = \frac{v_C}{R_0} + C_0 \frac{dv_C}{dt} \tag{4}$$

and the fault current can be written as

$$i_f = \frac{v_f}{R_f} = \frac{v_A}{R_f} \tag{5}$$

Using Equations (4) and (5), Equation (1) can be written as

$$i_N = \frac{v_A}{R_f} + \frac{v_A + v_B + v_C}{R_0} + C_0 \frac{d}{dt}(v_A + v_B + v_c). \tag{6}$$

For a balanced distribution network, the vector sum of three phase-to-neutral voltages will be zero. If phase-to-neutral voltages for Phases A, B, and C are represented by e_A, e_B, and e_C, respectively; it can be written as

$$e_A + e_B + e_C = 0. \tag{7}$$

By applying Kirchhoff's voltage law (KVL), the phase-to-ground voltage for each phase can be represented as the sum of the phase-to-neutral and neutral-to-ground voltages which can be written as follows:

$$v_A = e_A + v_N$$

$$v_B = e_B + v_N$$

$$v_C = e_C + v_N. \tag{8}$$

Since $e_A + e_B + e_C = 0$, $v_A + v_B + v_C$ can be obtained from Equation (8) and written as

$$v_A + v_B + v_C = 3v_N. \tag{9}$$

Using Equation (9), Equation (6) can be simplified as

$$i_N = \frac{v_A}{R_f} + 3\frac{v_N}{R_0} + 3C_0 \frac{dv_N}{dt}. \tag{10}$$

As indicated earlier on, the model is developed by considering an SLG fault on Phase A for which it is essential to calculate the neutral current in terms of the faulty phase voltage, i.e. v_A. Hence, v_N in Equation (10) needs to be replaced in terms of v_A and e_A which can be obtained from the first equation of the set of equations in Equation (8) and written as follows:

$$v_N = e_A - v_A. \tag{11}$$

Similarly, the model can be developed by considering faults on other phases and in that case, the neutral voltage needs to be expressed in terms of the corresponding phase-to-ground voltage. Substituting the value of v_N from Equation (11) into Equation (10), it can be written as

$$i_N = \left(\frac{3}{R_0} + \frac{1}{R_f}\right) v_A + 3C_0 \frac{dv_A}{dt} - \left(\frac{3}{R_0} e_A + 3C_0 \frac{de_A}{dt}\right). \tag{12}$$

The dynamic of the current flowing through the neutral in Equation (12) can be obtained applying KVL based on the loop from the neutral-to-ground while considering the output voltage of the RCC inverter. This dynamic can be represented as

$$\frac{di_N}{dt} = \frac{mV_{dc} - v_N}{L_p} \tag{13}$$

where V_{dc} is the total input voltage to the T-type RCC inverter and m is the modulation index or switching control input of the RCC inverter. The switching control signal m is regulated in such a way that the RCC inverter injects a current to the neutral which completely compensates the fault current and this will be possible if the reference value of the neutral current is selected as follows based on Equation (12):

$$i_{N_{ref}} = -\left(\frac{3}{R_0} e_A + 3C_0 \frac{de_A}{dt}\right). \tag{14}$$

The proposed NFT-SMC will inject the current as represented by Equation (14) in order to compensate the fault current and mitigate powerline bushfires. The detailed designed procedure for the NFT-SMC is presented in the following section along with a brief overview of the NT-SMC.

3 | PROPOSED SLIDING MODE CONTROLLER DESIGN FOR RCC INVERTERS

The selection of the sliding surface (SS) plays a significant role to design the sliding mode controller (SMC) as the performance of the controller depends on this surface. The desired performance can be achieved with an SMC if the SS is selected in such a way that it converges to zero in a finite time. The proposed NFT-SMC is designed in this section based on the dynamical model in Equation (13) where the main target is to determine m based on an NFT-SS as discussed in [18]. Here, the control input for the RCC inverter is obtained by satisfying the stability criteria of the system. Similarly, the NT-SMC is designed using the non-singular terminal sliding surface (NT-SS) as presented in [19, 20] as the performance of the NFT-SMC is compared with this controller. The design process of these controllers are discussed in the following subsections.

3.1 | NFT-SMC design for RCC inverters

The fast transient response without any singularity problems can be ensured and the desired control performance can only be achieved for an error ($e = i_N - i_{N_{ref}}$) if the following NFT-SS is selected [18]:

$$S_{NFT-SMC} = e + k_1 e^{\lambda} + k_2 \dot{e}^{\frac{p}{q}} \tag{15}$$

where $S_{NFT-SMC}$ denotes the NFT-SS; k_1 and k_2 are positive constants; and p and q are positive odd numbers which satisfy the condition, $1 < \frac{p}{q} < 2$ for avoiding the singularity problem [19, 20]; and $\lambda > \frac{p}{q}$ which is a positive constant used for ensuring the fast convergence [18].

As indicated earlier in this section, the NFT-SS as presented by Equation (15) requires to converge to zero ($S_{NFT-SMC} = 0$) within a finite time for ensuring the desired control performance, i.e. $e = 0$. Finally, the desired control law needs to be obtained by satisfying the stability criteria for the NFT-SS in Equation (15). To do this, the control Lyapunov function (CLF) can be selected as follows:

$$W_{NFT-SMC} = \frac{1}{2} S^2_{NFT-SMC} \tag{16}$$

where $W_{NFT-SMC}$ is the CLF and its derivative can be written as follows:

$$\dot{W}_{NFT-SMC} = S_{NFT-SMC} \dot{S}_{NFT-SMC}. \tag{17}$$

For ensuring the stability, $\dot{W}_{NFT-SMC} < 0$ or $\dot{W}_{NFT-SMC} \leq 0$ and thus, it is essential to calculate $\dot{S}_{NFT-SMC}$. This derivative can be obtained by taking the derivative of Equation (15) and written as follows:

$$\dot{S}_{NFT-SMC} = \dot{e} + k_1 \lambda |e|^{\lambda - 1} + \frac{k_2 p}{q} \dot{e}^{\frac{p}{q} - 1} \ddot{e} \tag{18}$$

where the values of $\dot{e}$ and $\ddot{e}$ can be calculated as follows:

$$\begin{aligned} \dot{e} &= \frac{1}{L_p}(mV_{dc} - v_N) - \dot{i}_{N_{ref}} \\ \ddot{e} &= \frac{1}{L_p}(\dot{m}V_{dc} - \dot{v}_N) - \ddot{i}_{N_{ref}}. \end{aligned} \tag{19}$$

The condition for the stability, i.e. $\dot{W}_{NFT-SMC} < 0$ or $\dot{W}_{NFT-SMC} \leq 0$ will be satisfied if and only if the following condition holds:

$$\begin{aligned} \dot{S}_{NFT-SMC} &= \dot{e} + k_1 \lambda |e|^{\lambda - 1} + \frac{k_2 p}{q} \dot{e}^{\frac{p}{q} - 1} \ddot{e} \\ &= -k_3 sgn(S_{NFT-SMC}) \end{aligned} \tag{20}$$

where k_3 is a large positive constant which is chosen to ensure the stability of the system and sgn represents a discontinuous signum function which can be written as

$$sgn(S_{NFT-SMC}) = \begin{cases} +1 & \text{if } S_{NFT-SMC} > 0 \\ 0 & \text{if } S_{NFT-SMC} = 0 \\ -1 & \text{if } S_{NFT-SMC} < 0. \end{cases} \tag{21}$$

Using the condition in Equation (20), Equation (17) can be written as

$$\dot{W}_{NFT-SMC} = -k_3 S_{NFT-SMC} sgn(S_{NFT-SMC}. \tag{22}$$

At this point, the control law can be obtained from Equation (20) by substituting the values of $\dot{e}$ and $\ddot{e}$ from Equation (19) which can be written as

$$\begin{aligned} \dot{m}_{NFT-SMC} = \frac{qL_p}{k_2 p |e|^{\frac{p}{q} - 1}} \Bigg[& \frac{\dot{v}_N}{L_p} + \ddot{i}_{N_{ref}} \\ & - \left(1 + k_1 \lambda |e|^{\lambda - 1}\right) \left(\frac{(mV_{dc} - v_N)}{L_p} - \dot{i}_{N_{ref}} \right) \\ & - k_3 sgn(S_{NFT-SMC}) \Bigg]. \end{aligned} \tag{23}$$

Here, $\dot{m}_{NFT-SMC}$ is considered as equivalent to $\dot{m}$ for the NFT-SMC. The discontinuous signum function in the control law in Equation (23) produces chattering which can be eliminated by introducing the following continuous function:

$$sgn(S_{NFT-SMC}) = \frac{S_{NFT-SMC}}{|S_{NFT-SMC}| + \epsilon} \tag{24}$$

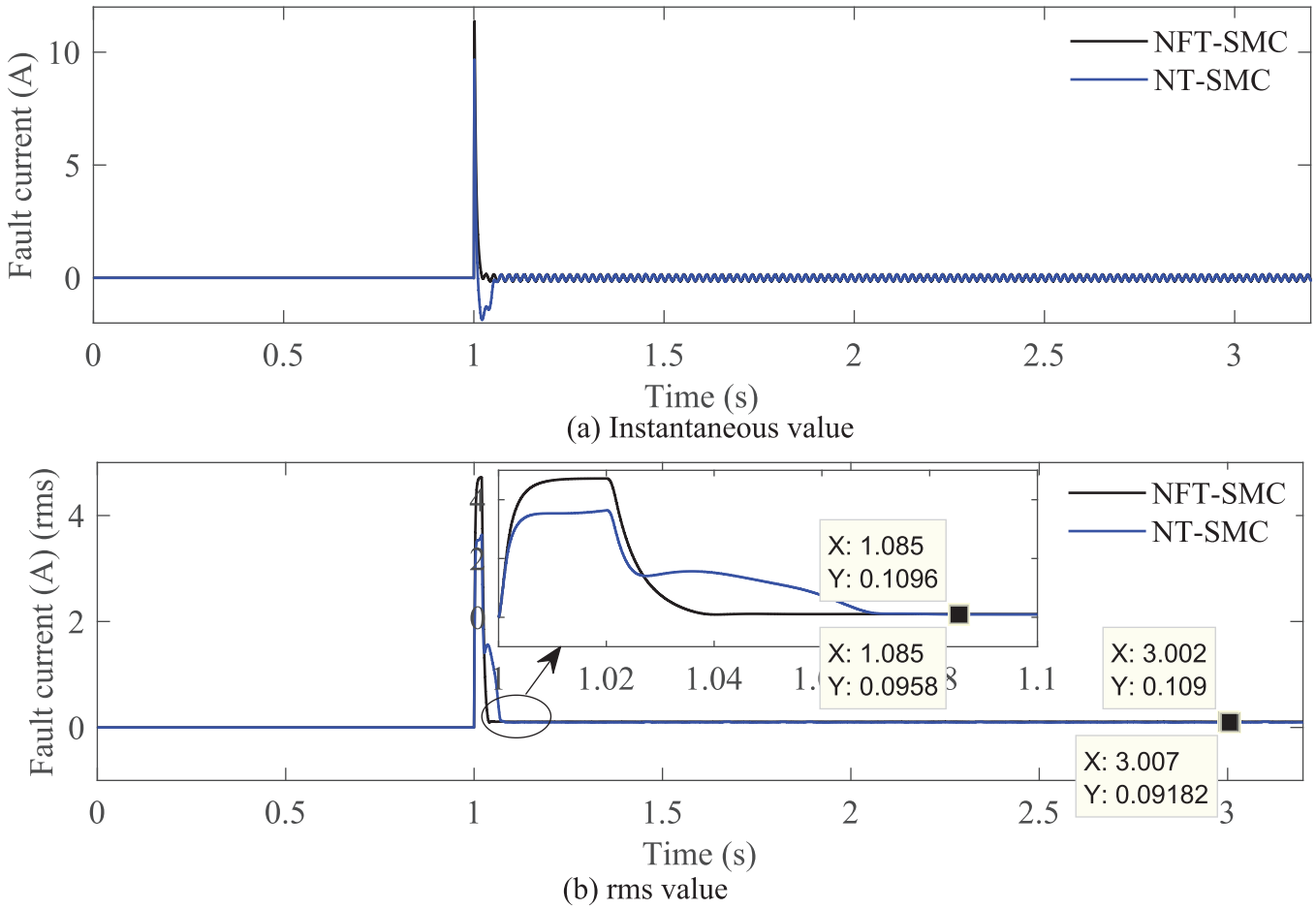

FIGURE 2 Fault current for $R_f = 400\ \Omega$ with an SLG fault on Phase A

where ϵ is a small positive number which is used to avoid the singularity problem for the condition $|S_{NFT-SMC}| = 0$. Using Equation (24), Equation (22) can be written as

$$\dot{W}_{NFT-SMC} = -k_3 \frac{S^2_{NFT-SMC}}{|S_{NFT-SMC}| + \epsilon} \leq 0 \tag{25}$$

which clearly indicates the stability under any circumstances. Hence, the final control law for the NFT-SS can be written as

$$\dot{m}_{NFT-SMC} = \frac{qL_p}{k_2 p |e|^{\frac{p}{q}-1}} \left[\frac{\dot{v}_N}{L_p} + \ddot{i}_{N_{ref}} - \left(1 + k_1 \lambda |e|^{\lambda-1}\right) \left(\frac{(mV_{dc} - v_N)}{L_p} - \dot{i}_{N_{ref}} \right) - k_3 \frac{S^2_{NFT-SMC}}{|S_{NFT-SMC}| + \varepsilon} \right]. \tag{26}$$

This control input is used for the RCC inverter to ensure the fast convergence of the error, i.e. the desired tracking of the neutral current. The following subsection presents the controller design process for an NT-SMC as the performance of the NFT-SMC is compared with this controller.

3.2 | NT-SMC design for RCC inverters

The transient response without facing any singularity issues can be achieved for an error (e) if the following non-singular terminal sliding surface (NT-SS) is selected [18]:

$$S_{NT-SMC} = \dot{e} + k_4 e^{\frac{p}{q}} \tag{27}$$

where S_{NT-SMC} represents the NT-SS and k_4 is a positive constant.

For analysing the convergence of the sliding surface and error, the CLF (W_{NT-SMC}) can be selected as follows:

$$W_{NT-SMC} = \frac{1}{2} S^2_{NT-SMC} \tag{28}$$

and its derivative can be written as follows:

$$\dot{W}_{NT-SMC} = S_{NT-SMC} \dot{S}_{NT-SMC}. \tag{29}$$

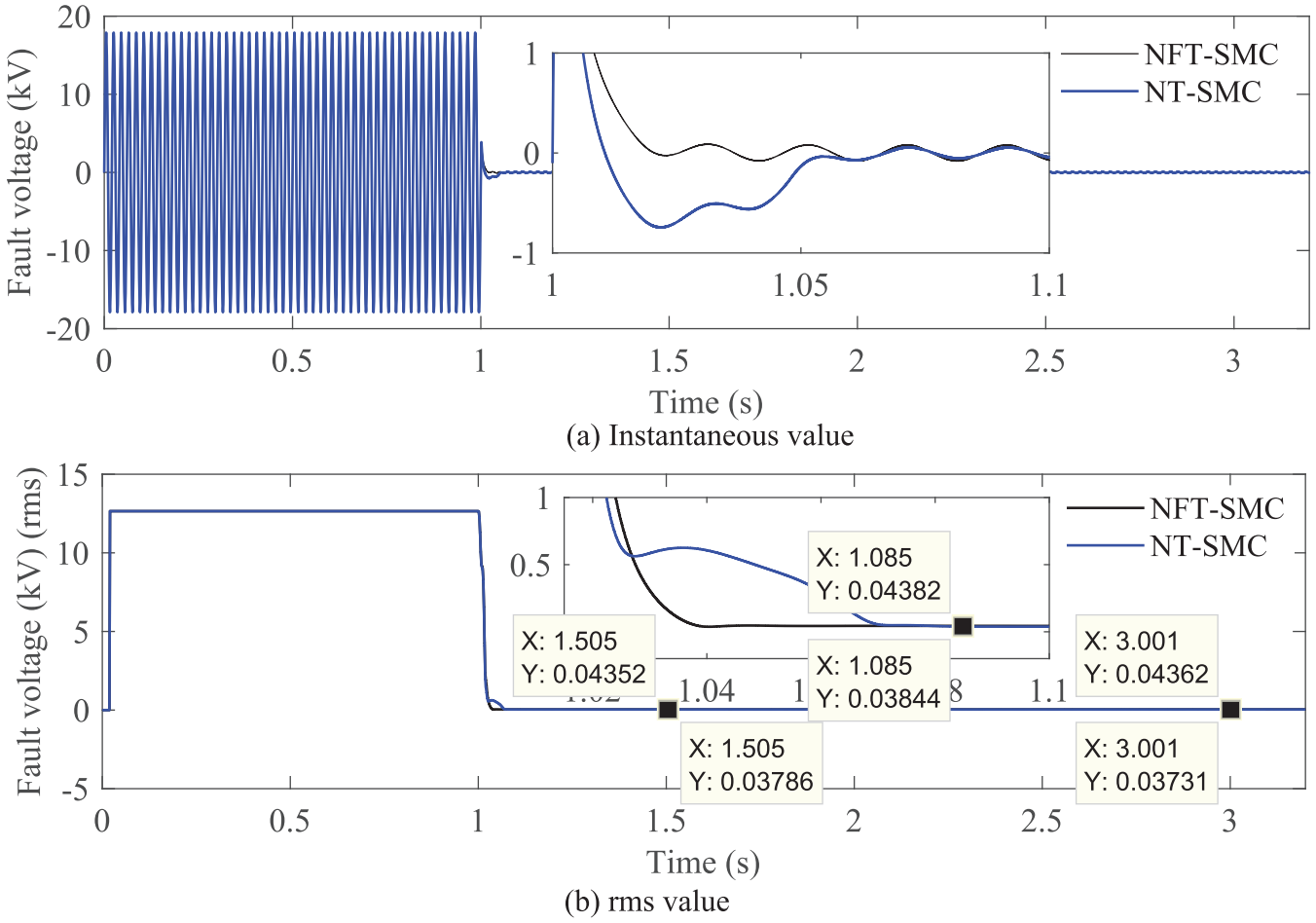

FIGURE 3 Faulty phase voltage for $R_f = 400\ \Omega$ with an SLG fault on Phase A

For ensuring the stability, $\dot{W}_{NT-SMC}$ can be obtained by taking the derivative of Equation (27) and written as follows:

$$\dot{S}_{NT-SMC} = \ddot{e} + \frac{k_4 p}{q}|e|^{\frac{p}{q}-1}\dot{e}. \tag{30}$$

The condition for the stability will be satisfied if and only if the following condition holds:

$$\begin{aligned}\dot{S}_{NT-SMC} &= \ddot{e} + \frac{k_4 p}{q}|e|^{\frac{p}{q}-1}\dot{e} \\ &= -k_5 sgn(S_{NT-SMC})\end{aligned} \tag{31}$$

where k_5 is a large positive constant which is chosen to ensure the stability of the system and sgn represents a discontinuous signum function as discussed in the previous subsection. Using the condition in Equation (31), Equation (29) can be written as

$$\dot{W}_{NT-SMC} = -k_5 S_{NT-SMC} sgn(S_{NFT-SMC}). \tag{32}$$

At this instant, the control law can be obtained from Equation (31) by substituting the values of $\dot{e}$ and $\ddot{e}$ from Equation (19) which can be written as

$$\begin{aligned}\dot{m}_{NT-SMC} = \frac{L_p}{V_{dc}}\Bigg[&\frac{\dot{v}_N}{L_p} + \ddot{i}_{N_{ref}} - \frac{k_4 p}{q}|e|^{\frac{p}{q}-1} \\ &\left(\frac{V_{dc}}{L_p}m - \frac{v_N}{L_p} - \dot{i}_{N_{ref}}\right) - k_5 sgn(S_{NT-SMC})\Bigg].\end{aligned} \tag{33}$$

Here, $\dot{m}_{NT-SMC}$ is considered as equivalent to $\dot{m}$ for the NT-SMC. The chattering effects due to the discontinuous signum function in Equation (33) can be eliminated by introducing the following continuous function:

$$sgn(S_{NT-SMC}) = \frac{S_{NT-SMC}}{|S_{NT-SMC}| + \sigma} \tag{34}$$

where σ is a small positive number which is used to avoid the singularity problem for the condition $|S_{NT-SMC}| = 0$. Using

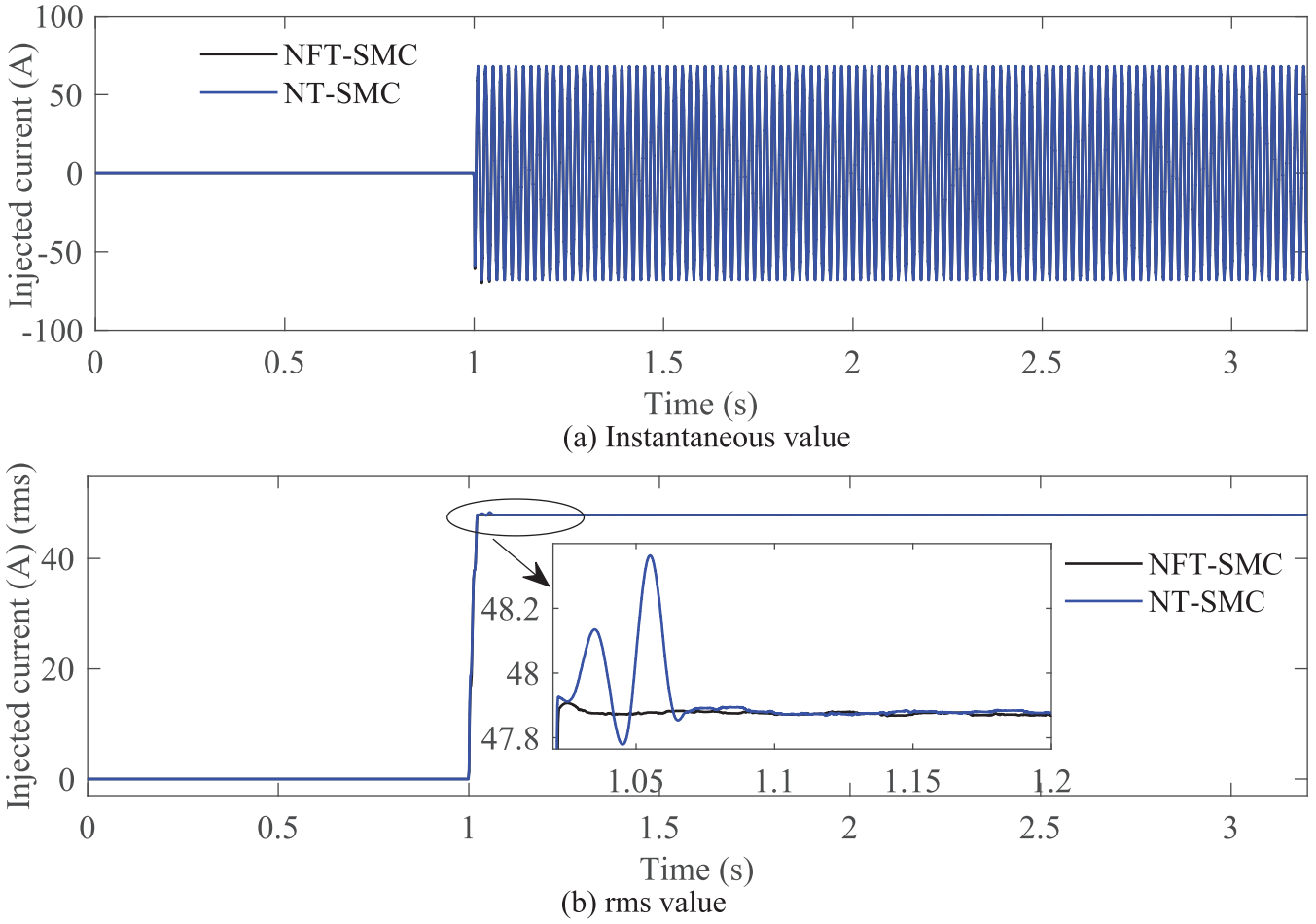

FIGURE 4 Injected current by the RCC inverter for $R_f = 400\ \Omega$ with an SLG fault on Phase A

Equation (34), Equation (32) can be written as

$$\dot{W}_{NT-SMC} = -k_5 \frac{S^2_{NT-SMC}}{|S_{NT-SMC}| + \sigma} \leq 0 \tag{35}$$

which means the system is stable. Hence, the final control law for the NT-SS can be written as

$$\dot{m}_{NT-SMC} = \frac{L_p}{V_{dc}} \left[\frac{\dot{v}_N}{L_p} + \ddot{i}_{N_{ref}} - \frac{k_4 p}{q} |e|^{\frac{p}{q}-1} \left(\frac{V_{dc}}{L_p} m - \frac{v_N}{L_p} - \dot{i}_{N_{ref}} \right) - k_5 \frac{S_{NT-SMC}}{|S_{NT-SMC}| + \sigma} \right]. \tag{36}$$

This control input is used for the RCC inverter to ensure the fast convergence of the error, i.e. the desired tracking of the neutral current. The following section shows some case studies to compare the performances of NFT-SMC and NT-SMC in compensating the fault current and faulty phase voltage for an SLG fault in a compensated distribution network with an aim to reduce the likelihood of powerline bushfires.

4 | SIMULATION RESULTS

The compensated distribution network as shown in Figure 1 is the test system used in this paper to verify the performance of the NFT-SMC and NT-SMC in maintaining the fault current and faulty phase voltage to zero through the action of the controller within the RCC inverter. Simulations are carried out in a way that the fault current is compensated by the RCC inverter with the designed NFT-SMC in order to mitigate the devastating effects of powerline bushfires. The test network and performance requirement for the controller as well as the control system parameters are discussed next.

4.1 | Test network

The Simulink platform is used to develop the test network as well as design and test the effectiveness of the control laws. The voltage level is taken as 22 kV line-to-line (rms) which is the voltage of the distribution feeder where the REFCL is being implemented in Victoria, Australia [17]. The rate phase-to-neutral voltage is 12.7 kV (rms) which is also the

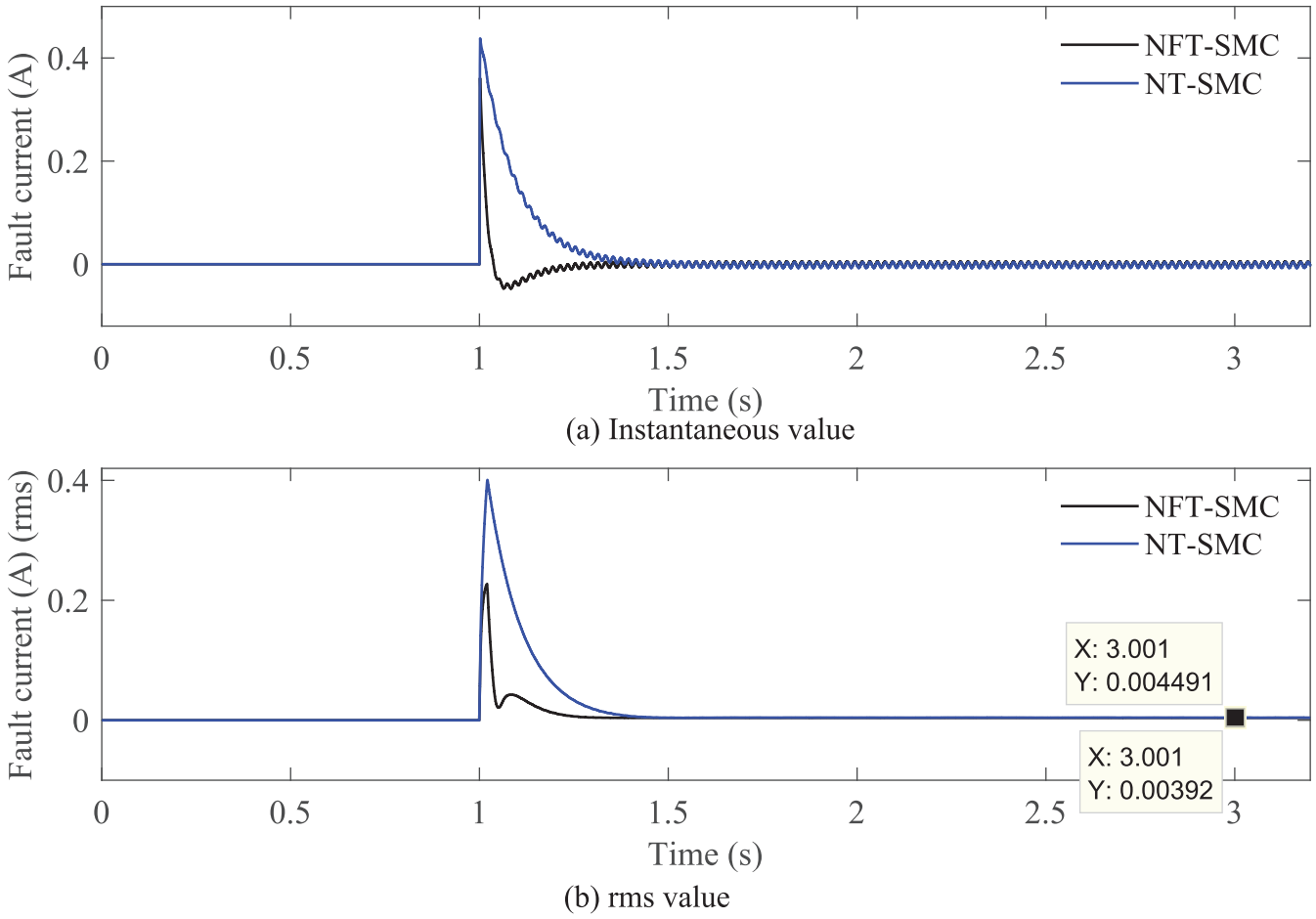

FIGURE 5 Fault current for $R_f = 1.3\ \text{k}\Omega$ with an SLG fault on Phase A

phase-to-ground voltage if the neutral-to-ground voltage is kept to a very low value by minimising the imbalance current in the distribution network for the REFCL operation. The value of the adjustable inductor (L_p) is considered as 0.9 H based on the line parameters to make the resonance condition while the zero-sequence resistance and capacitance for each phase is considered as 28 kΩ and 4 μF, respectively as the distribution network is considered as a balanced system. The load is connected between two phases whose value for each phase-to-phase is considered as 400 Ω. Figure 1 also shows that two 400 V dc sources are considered as the input.

4.2 | Performance requirements

The faulty phase voltage and fault current need to be compensated within certain time frames guided by the operational standard in [17] to reduce the risk of bushfire resulting from SLG powerline faults. According to this standard, the value of the fault current should maintained at a value lower than 0.5 A within 2 s of activating the RCC inverter for both high impedance ($R_f \geq 1\ \text{k}\Omega$) and low impedance ($R_f < 1\ \text{k}\Omega$) faults. At the same time, the faulty phase voltage needs to be reduced to a value equals to or lower than 1.9 kV, 0.75 kV, and 0.25 kV within 0.085 s, 0.5 s, and 2 s, respectively after activating the RCC inverter for the low impedance fault. For high impedance faults, this voltage is only observed at 2 s after starting the compensation with the RCC inverter and its value needs to be maintained at a value equals to or lower than 0.25 kV. It is worth noting that the RCC inverter comes into operation at the instant of detecting the SLG fault using the neutral voltage.

4.3 | Control implementation and parameters

The performances of the designed NFT-SMC and NT-SMC are analysed against the performance requirements as discussed in the previous subsection with a focus to compensate the fault current and mitigate powerline bushfires. Equation (26) is developed in MATLAB/SIMULINK platform and then integrated design the switching control input in the instantaneous form and the PWM scheme is used for generating the actual switching pulses for switches used in the RCC inverter. Here, the switching frequency for the RCC inverter is considered as

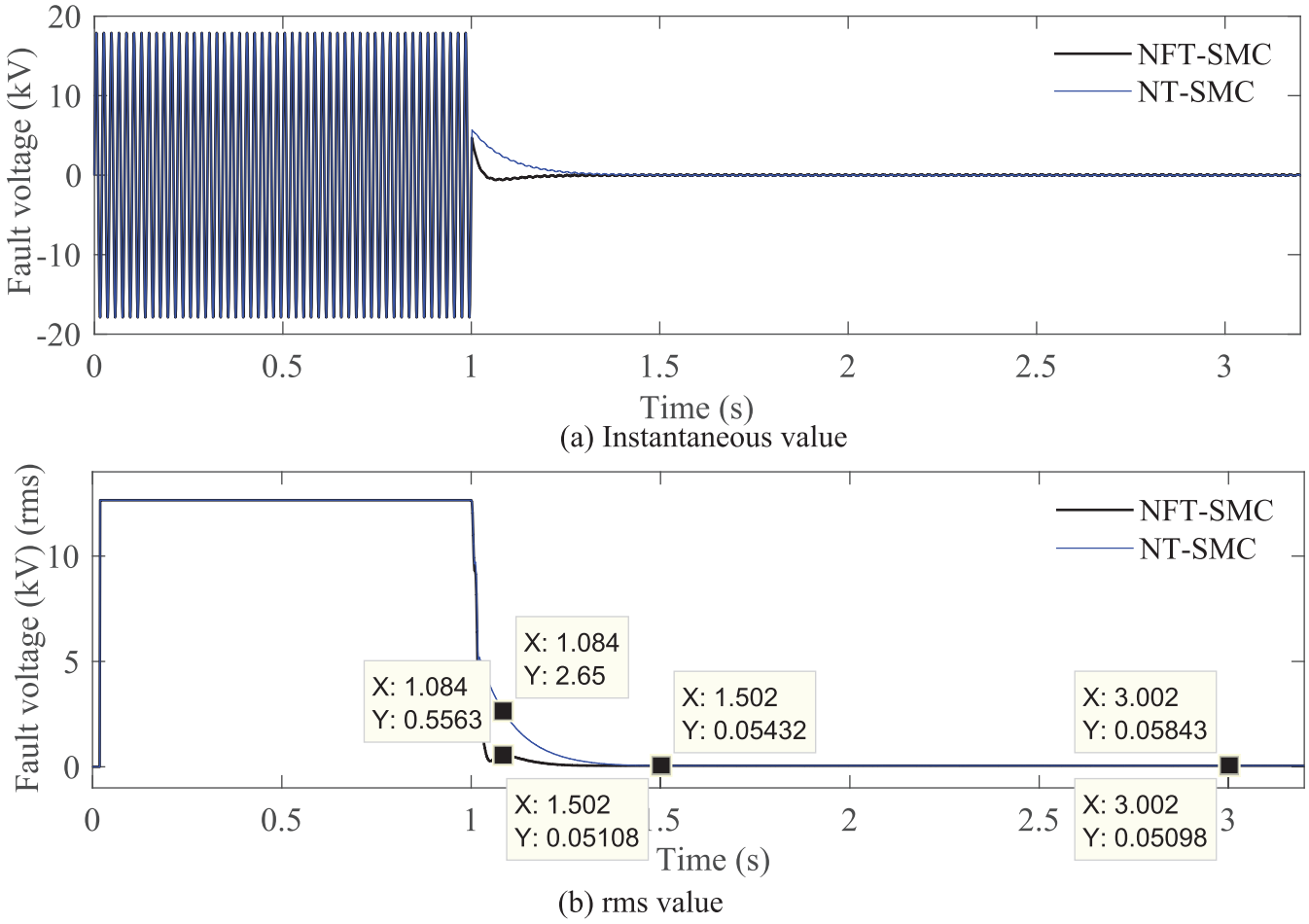

FIGURE 6 Faulty phase voltage for $R_f = 1.3\ \text{k}\Omega$ with an SLG fault on Phase A

10 kHz. The switching signal for the NT-SMC is also designed in a similar way based on Equation (36). The simulation studies are performed by considering the control parameters for the NFT-SMC as: $p = 5$, $q = 3$, $k_1 = 8500$, $k_2 = 450$, $\lambda = 1.8$ and $\epsilon = 0.5$ and for the NT-SMC as $p = 5$, $q = 3$, $k_4 = 8500$, $k_5 = 450$, and $\sigma = 0.5$.

4.4 | Case studies

The performance of the proposed controller is evaluated by applying an SLG fault on phase A of the network with varying fault resistance, R_f. A low impedance fault scenario with fault resistance of 400 Ω and two high resistance fault scenarios with fault resistances of 1.3 kΩ and 25.4 kΩ are explored to compare the fault current compensation capabilities of the NFT-SMC and NT-SMC. The fault is applied at 1 s and the operation of the RCC inverter is initiated at the same time that reflects the fast response requirement for bushfire mitigation. The performances of the controllers are analysed and compared for these three different values of the fault resistances which are reflected through three case studies as discussed below.

- **Case 1**: Controller performance evaluation for $R_f = 400\ \Omega$

In this case, a low impedance SLG fault is applied on Phase A where the fault resistance is 400 Ω, i.e. $R_f = 400\ \Omega$. The instantaneous and rms fault currents are shown in Figure 2 from where it is clear that both NFT-SMC and NT-SMC act to reduce the fault current to the targeted value of 0.5 A within 2 s after the RCC inverter has been activated. In fact, the fault current becomes around 0.1 A by the action of any of the controllers as shown in the rms representation of the fault current [see Figure 2(b)]. However, the NFT-SMC acts quicker than the NT-SMC as is evident from the inset of Figure 2(b). The instantaneous and rms values of the faulty phase voltage, i.e. the phase-to-ground voltage for Phase A are shown in Figure 3. The faulty phase voltages of the network using the NFT-SMC with the RCC inverter are 38.44 V, 37.86 V, and 37.31 V at 85 ms, 0.5 s, and 2 s, respectively, after the RCC inverter compensation takes place. Furthermore, the corresponding voltages with the NT-SMC are 43.82 V, 43.52 V, and 43.62 V. Hence, it is clear from the responses that both controllers are able to satisfy the requirements of reducing the voltage within specified time frames. However, the control action of the NFT-SMC

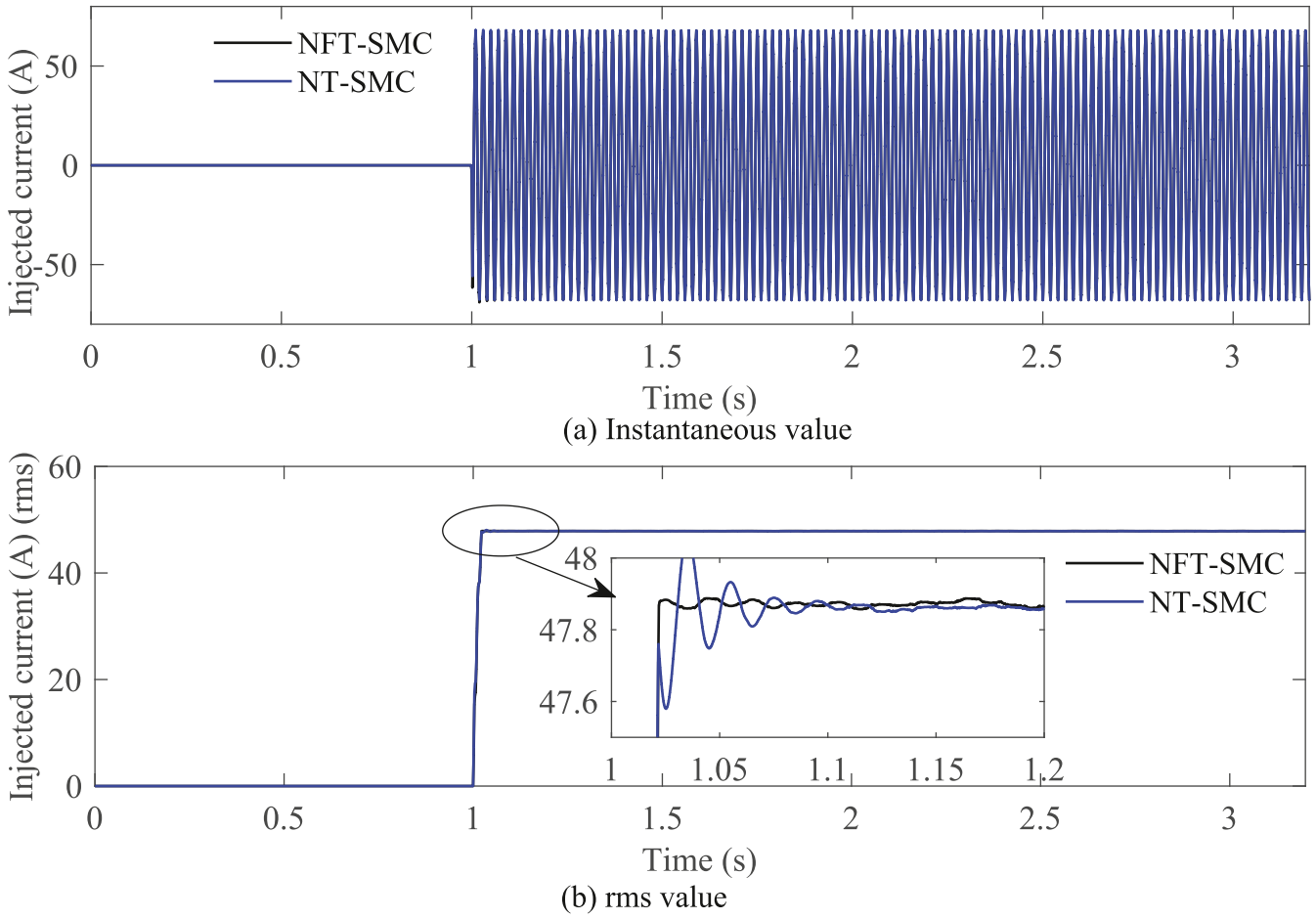

FIGURE 7 Injected current by the RCC inverter for $R_f = 1.3\ \text{k}\Omega$ with an SLG fault on Phase A

reduces the fault voltage faster as compared with the NT-SMC, as seen from the inset of Figure 3(b). Surprisingly, the fault voltage somewhat slightly increases at 2 s from 0.5 s for the NT-SMC case. Therefore, it can be summarised that the NFT-SMC achieves the performance requirements for the compensated distribution network faster than the NT-SMC which is also evident from the injected current from the RCC inverter as shown in Figure 4. The transient in the injected current for the NFT-SMC is smoother than that of the NT-SMC, making the NFT-SMC act quicker than the NT-SMC.

- **Case 2**: Controller performance evaluation for $R_f = 1.3\ \text{k}\Omega$

In this case, the fault resistance is $R_f = 1.3\ \text{k}\Omega$ with the SLG fault applied on the same phase, i.e. Phase A. This case is an illustration of high impedance fault in the compensated distribution system along with the corresponding actions of the designed NFT-SMC as compared to the NT-SMC. As in the previous case, both controllers are able to reduce the fault current to less than 0.5 A within 2 s of the fault occurrence which is illustrated in Figure 5. This current reduction is achieved through the action of the RCC inverter which is controlled by the NFT-SMC or NT-SMC. The fault current is significantly lower than the previous case because of significantly higher fault resistance. The fault current is reduced to 0.004 A for both of the controllers at 3 s which is 2 s after the fault is applied. The differences in the performance of the controllers are seen from the rms representation of the fault current, similar to the situation in Case 1. It is clear that the NFT-SMC outperforms the NT-SMC in terms of compensating the fault current by reducing the fault current faster. The voltage responses of both controllers for the compensated distribution network are shown in Figure 6. At 85 ms after the RCC inverter is applied, the fault voltage reduces to 55.63 V by the application of the NFT-SMC, however, the voltage is almost five times higher (2.65 kV) where the NT-SMC is applied. Afterwards, the fault voltages at 0.5 s and 2 s after the RCC inverter compensation starts become 51.08 V and 50.98 V, respectively, for the NFT-SMC and 54.32 V and 58.43 V, respectively, for the NT-SMC. Here, again the fault voltage increases at 2 s compared to the same at 0.5 s in the case where the RCC inverter is controlled by the NT-SMC. The injected current by the RCC inverter as shown in Figure 7 further validates the fault current compensation capability of the NFT-SMC and demonstrates its

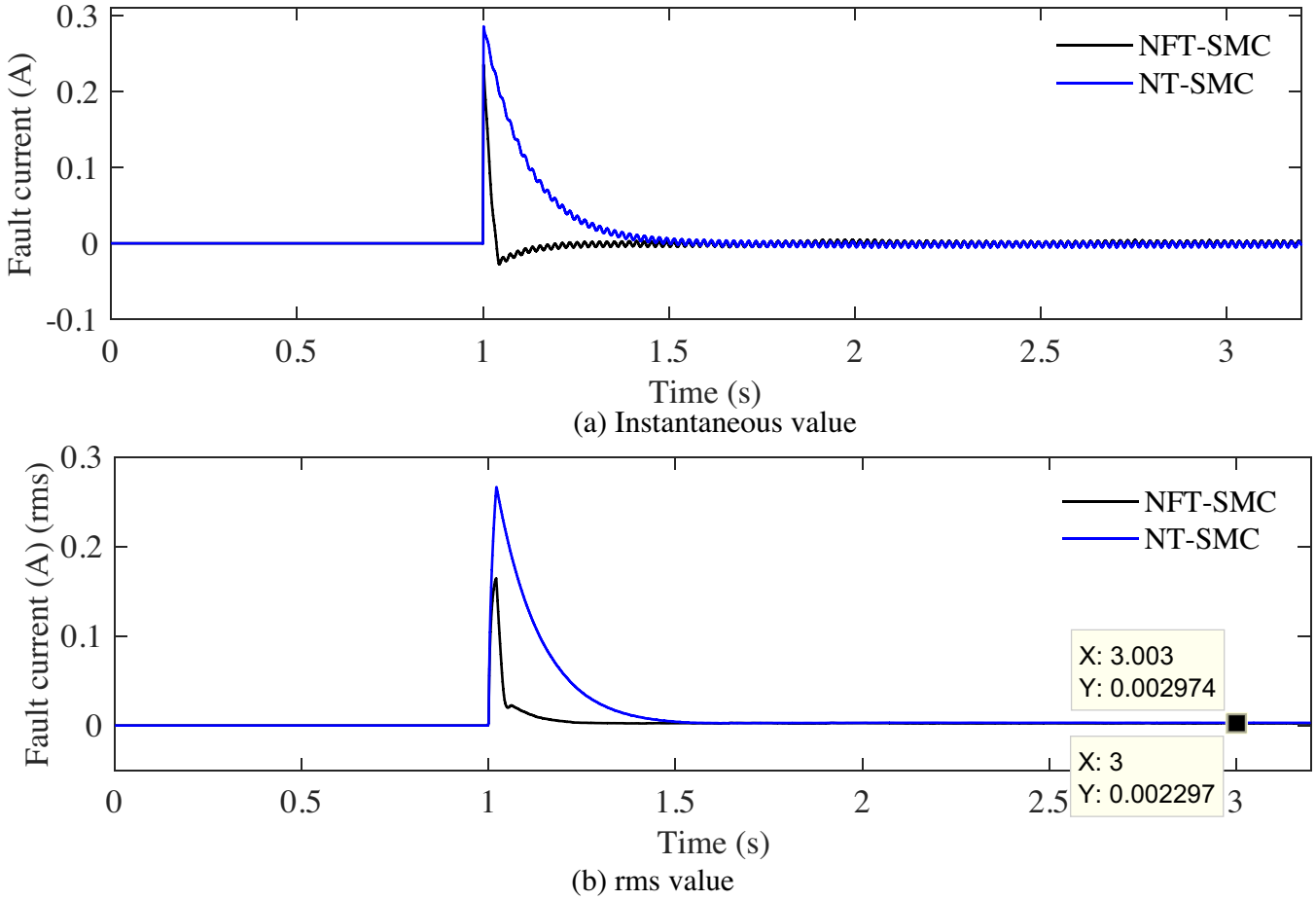

FIGURE 8 Fault current for $R_f = 25.4\ \text{k}\Omega$ with an SLG fault on Phase A

superiority over the NT-SMC. Hence, the NFT-SMC enables the RCC inverter to effectively compensate both low and high impedance faults.

- **Case 3**: Controller performance evaluation for $R_f = 25.4\ \text{k}\Omega$

Finally, another high impedance fault scenario is simulated with $R_f = 25.4\ \text{k}\Omega$. Here, the highest value of the fault resistance that the need to be detected in the compensated distribution system is considered to further validate the performance of the NFT-SMC through simulation results. The fault currents in the network compensated through the control actions of the NFT-SMC and NT-SMC are shown in Figure 8 for both the instantaneous and rms values. As in the previous two cases, the fault current compensation requirements are met for both of the controllers and the NFT-SMC acts faster than the NT-SMC. The faulty phase voltage responses in Figure 9 are also similar to the two previous cases. The transient response of the NFT-SMC is better than that of the NT-SMC. The injected current by the RCC inverter is shown in Figure 10 which shows less oscillations, i.e. better settling performance, in the injected current.

4.5 | Performance summary

In summary, the designed controller is able to fulfil the fault current compensation requirements for the compensated distribution network to mitigate powerline bushfires. Moreover, the faulty phase voltage compensation requirements at different time frames are also met which limits the thermal energy emitted during an SLG fault resulting in devastating bushfires generated from powerlines. The designed controller not only satisfies the performance requirements to reduce the likelihood of powerline initiated bushfires but also outperforms existing controller, e.g. NT-SMC, as demonstrated through three case studies considering both low and high impedance faults. Hence, the designed NFT-SMC can be applied to control the RCC inverter in compensated distribution networks and reduce the risk of powerline bushfires more significantly.

5 | CONCLUSION

The non-singular fast terminal sliding mode control scheme is employed to derive the switching control input for the RCC inverter in a compensated distribution network. A non-singular

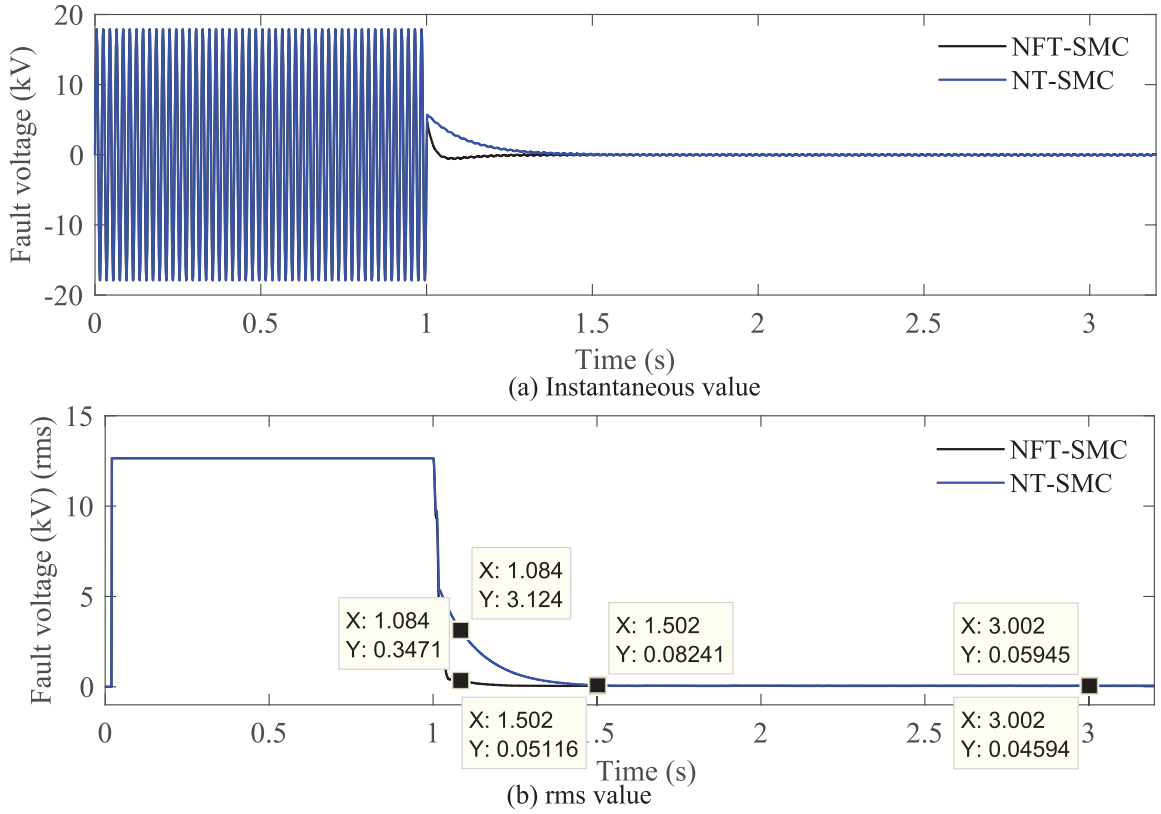

FIGURE 9 Faulty phase voltage for $R_f = 25.4\ \text{k}\Omega$ with an SLG fault on Phase A

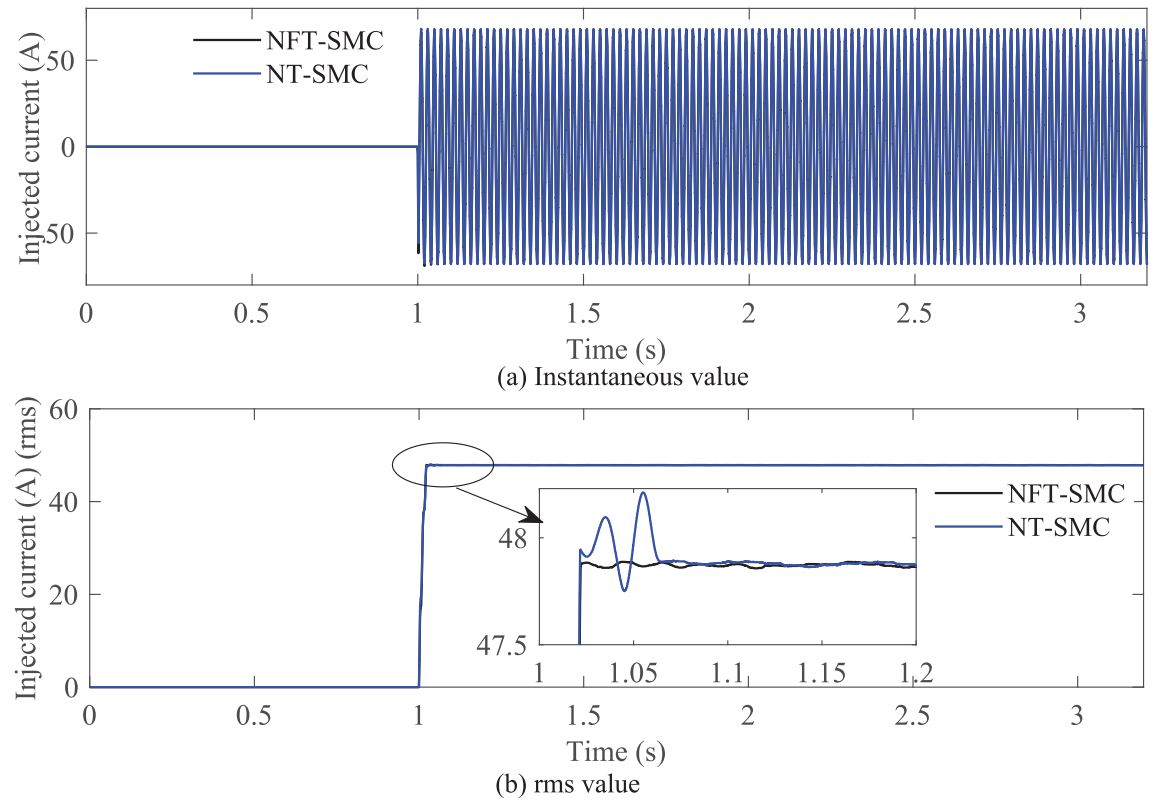

FIGURE 10 Injected current by the RCC inverter for $R_f = 25.4\ \text{k}\Omega$ with an SLG fault on Phase A

fast terminal sliding surface is used to ensure the fast convergence of the neutral current tracking error so that the fault current is eliminated and the fault phase voltage is maintained within a limit which are important for mitigating powerline bushfires. The designed non-singular fast terminal sliding mode controller eliminates the chattering effects as it uses a continuous function rather than the discontinuous signum function that is used for traditional sliding mode controllers. Since the dynamic of the RCC inverter is simple and the sliding mode controller has better tracking characteristics for the sinusoidal reference, the designed controller quickly enforces the error within the sliding surfaces and initiates the fault current compensation which has further proven through simulation results under different fault resistances. The designed controller provides better compensation of the fault current and thus, reduces the risk of powerline bushfires in a much faster way than the non-singular terminal sliding mode controller. This is due to the inclusion of some additional features, helping to improve the convergence speed, in the non-singular fast terminal sliding surface while comparing with the non-singular terminal sliding surface. The designed controller does not consider the effects of parametric uncertainties and external disturbances though these are key inherent features of the sliding mode control scheme and the future works will consider these features to design controllers for the similar system.

ORCID


Tushar Kanti Roy https://orcid.org/0000-0002-1992-0881

REFERENCES

1. Teague, B., McLeod, R., Pascoe, S.: 2009 Victorian Bushfires Royal Commission. [Final Report]Parliament of Victoria (2010)
2. Orton, T.: Powerline Bushfire Safety Taskforce: Final Report. [Final Report]Energy Safe Victoria (2011)
3. IEEE recommended practice for grounding of industrial and commercial power systems. IEEE Std 142-2007 (Revision of IEEE Std 142-1991) 1–225 (2007)
4. Janssen, M., et al.: Residual current compensation (RCC) for resonant grounded transmission systems using high performance voltage source inverter. In: 2003 IEEE PES Transmission and Distribution Conference and Exposition (IEEE Cat. No.03CH37495). vol. 2. (2003). pp. 574–578
5. Qi, M., et al.: Fast disposal method for reducing electricity risk of single-phase ground fault in distribution network. In: 2017 China International Electrical and Energy Conference (CIEEC). pp. 554–558. (2017)
6. Wang, F., Guo, M., Yang, G.: Novel arc-suppression methods based on cascaded H-bridge converter. In: 2016 Asia-Pacific International Symposium on Electromagnetic Compatibility (APEMC). vol. 1, pp. 691–694. (2016)
7. Zheng, Z.Y., et al.: Flexible arc-suppression method based on improved distributed commutations modulation for distribution networks. Int. J. Electr. Power Energy Syst. 116, 105580 (2020)
8. Gargoom, A., et al.: Residual current compensator based on voltage source converter for compensated distribution networks. In: 2018 IEEE Power Energy Society General Meeting (PESGM). pp. 1–5 (2018)
9. Wang, W., et al.: Control method of an arc suppression device based on single-phase inverter. In: 2016 International Symposium on Power Electronics, Electrical Drives, Automation and Motion (SPEEDAM). pp. 929–934. (2016)
10. Chen, D., et al.: Active inverter device with double closed loop control method for arc suppression in distribution network. In: 2017 China International Electrical and Energy Conference (CIEEC). pp. 549–553. (2017)
11. Wang, W., et al.: Principle and design of a single-phase inverter-based grounding system for neutral-to-ground voltage compensation in distribution networks. IEEE Trans. Ind. Electron. 64(2), 1204–1213 (2017)
12. Wang, W., et al.: Principle and control design of active ground-fault arc suppression device for full compensation of ground current. IEEE Trans. Ind. Electron. 64(6), 4561–4570 (2017)
13. Qiu, W., et al.: Model-predictive-control-based flexible arc-suppression method for earth fault in distribution networks. IEEE Access 7, 16051–16065 (2019)
14. Qu, Y., Tan, W., Yang, Y.: H-infinity control theory apply to new type arc-suppression coil system. In: 2007 7th International Conference on Power Electronics and Drive Systems. pp. 1753–1757. (2007)
15. Zheng, Z., et al.: FASD based on BSC method for distribution networks. IET Gener. Transm. Distrib. 13(24), 5487–5494 (2019)
16. Zheng, Z.Y., et al.: Single-phase flexible arc suppression device based on BSC-SOGI-PLL method for distribution networks. Int. J. Electr. Power Energy Syst. 121, 106100 (2020)
17. Acil Allen Consulting Pty Ltd: Regulatory Impact Statement: Bushfire Mitigation Regulations Ammendment. Department of Economic Development, Jobs, Transport and Resources. (2015)
18. Yang, L., Yang, J.: Nonsingular fast terminal sliding-mode control for nonlinear dynamical systems. Int. J. Robust Nonlinear Control 21(16), 1865–1879 (2011)
19. Feng, Y., Yu, X., Man, Z.: Non-singular terminal sliding mode control of rigid manipulators. Automatica 38(12), 2159–2167 (2002)
20. Chen, S., Lin, F.: Robust nonsingular terminal sliding-mode control for nonlinear magnetic bearing system. IEEE Trans. Control Syst. Technol. 19(3), 636–643 (2011)

How to cite this article: Roy TK, Mahmud MA, Nasiruzzaman ABM, Barik MA, Oo AMT. A non-singular fast terminal sliding mode control scheme for residual current compensation inverters in compensated distribution networks to mitigate powerline bushfires. *IET Gener Transm Distrib.* 2021;15:1421–1434.
https://doi.org/10.1049/gtd2.12110